Journal of Engineering and Applied Sciences 13 (4): 919-925, 2018
ISSN: 1816-949X


# Fabrication and Enhancement of SnS:Ag/Si Solar Cell via. Thermal Evaporation Technique

Khalid Haneen Abass, Anmar Adil and Musaab Khudhur Mohammed
Department of Physics, College of Education for Pure Sciences, University of Babylon, Hillah, Iraq

**Abstract:** In this rsearch, pure tin Sulfide (SnS) and 20 nm Ag nanoparticle-doped SnS (0.002, 0.004 and 0.006 wt.%) thin films are prepared by thermal evaporation technique with thickness of 75 nm. The X-Ray Diffraction (XRD) result showed that, the prepared films are polycrystalline with orthorhombic structure and preferential orientation in the 111 direction. The crystallite size refer to the quantization confinement effect that calculated from Scherer's formula, it increased with increasing of Ag doping. From Scanning Electron Microscopy (SEM) and Atomic Force Microscopy (AFM), the films morphology and surface roughness were affected by low Ag doping. The optical measurements of the films are studied by UV-visible spectrophotometer in the wavelength range 300-900 nm. The transmittance decreased with the increasing of Ag doping while the absorbance increased. The optical measurement shows that, the films are allowed direct Energy gap ($E_g$) that decreased from 3-2 eV with increasing of Ag-doping, the values of energy gaps refer to the confinement effect. The electrical properties of the films have been studied and found that the prepared films are p-type and carrier concentration (n) and electrical conductivity ($\sigma$) increased with the increasing of Ag doping. I-V characteristics show that, the Ag-doping increases the energy conversion efficiency by retarding the electron-hole recombination and the improved device performance caused by the high short-circuit current ($I_{sc}$) and open circuit Voltage ($V_{oc}$) and found that the highest efficiency ($\eta$) at doping 0.006 wt.% is 4.42% with ($V_{oc}$) of 2.5 V ($I_{sc}$) of 7 mA $cm^{-2}$ and Fill Factor (F.F) of 0.25 at intensity p =100 $mW/cm^2$.

**Key words:** SnS:Ag, thermal evaporation, optical properties, solar cell, efficiency, factor

## INTRODUCTION

In this view, it is necessary to focus our research on new photovoltaic materials which makes solar cell cheaper, more efficient and produces significantly more energy over its life time. One such material is tin Sulfide (SnS). It has interesting optical properties which is suitable to be used in photovoltaic applications. It is a IV-VI compound semiconductor material (Bushra and Ikhlas, 2014). SnS are very promising materials because of their attractive physical properties which can be controlled by changing the chemical composition which makes these materials useful for technological applications such as photovoltaic (Henry *et al*., 2013), solar cells (Reddy *et al*., 2006) and optoelectronic devices because of its favorable optical band gap energy of 1.35 eV, near optimum for photovoltaic solar energy conversion and high optical absorption coefficient $>10^4$/cm and a high photoelectric conversion efficiency. Additionally, it has the advantage that its constituents are made up of inexpensive, non-toxic and earth abundant elements. It exhibits both p and n-type conductivity depending on the tin and sulfur concentration and with temperature treatment (Bushra and Ikhlas, 2014). SnS thin films have been prepared using different methods such as thermal evaporation (Sajeesh *et al*., 2010), electro deposition (Mariappan *et al*., 2011), spray pyrolysis (Reddy *et al*., 2001), Pulsed Laser Deposition (PLD) (Vidal *et al*., 2012), sputtering (Hartman *et al*., 2011), vacuum evaporation (Blaesser and Roosi, 1988), Photo Electrochemical (PEC) (Avellaneda *et al*., 2007) and Chemical Bath Deposition (CBD) (Ghosh *et al*., 2008). In this study, thin films are prepared from pure and Ag-doped SnS by thermal evaporation technique and study the structural, morphological, optical and electrical properties and fabrication of SnS:Ag/Si heterojunction for photovoltaic application.

## MATERIALS AND METHODS

Fabrication and investigation of pure SnS and 20 nm Ag-doped SnS thin films with different doping concentration (0.002, 0.004 and 0.006) wt.% by thermal evaporation method on glass and silicon substrates.

**Corresponding Author:** Khalid Haneen Abass, Department of Physics, College of Education for Pure Sciences, University of Babylon, Hillah, Iraq

The thermal evaporation system is Edward C-306 deposition. The SnS powder with 99.9% purity and the Ag nanoparticle grains with 99.9% purity were used as source materials molybdenum boat. The chamber was evacuated down to $1\times10^{-7}$ mbar. The source to substrate distance was about 15 cm. The films were annealed at temperature of 473 K for 2 h. The structure of the films was characterized by a Shimadzu X-ray diffracts meter system (XRD-6000) with a source $CuK_{\alpha}$ with radiation of wavelength $\lambda$ = 1.5406 Å. The surface roughness was analyzed by a Aα3000 scanning probe microscope (AFM), Scanning Electron Microscope (SEM, JEOL JSM 6300). Spectrophotometer (Shimadzu UV-1650 PC) made by Phillips, (Japanese company) used to recorde transmission scales of the SnS:Ag thin films in the wavelength range of 300-900 nm. Based on Van der Pau method, the electrical properties were determined by a HMS 3000 Hall measurement system and the thickness of the films was measured by optical thin film measurement with Lambda Limf-10 and it was 75 nm.

## RESULTS AND DISCUSSION

The XRD pattern for pure and Ag-doped SnS films are shown in Fig. 1. From the XRD pattern, a peak was obtained at 2Θ = 31.71° which corresponds to the 111 reflection plane for pure SnS and other medium intensity peaks with different doping of Ag (0.002, 0.004, 0.006) wt.% at thicknesses of 75 nm are listed in Table 1. The diffraction peaks are attributed to SnS taken from the Joint Committee of Powder Diffraction Standard (JCPDS: 39-0354) and films are polycrystalline with the orthorhombic structure which is in good agreement with the finding of other researches by Henry *et al.* (2015). This implies that the particles are SnS with a strong 111 reflection plane. The preferred orientation of the particle is due to the fact that the growth process is controlled by nucleation. The result is also in agreement with the finding of other researches by Peng *et al.* (2007). A Full-Width at Half Maximum (FWHM) of the pure SnS and Ag-doped SnS films decreased slightly with the increasing of Ag-doped. This finding indicated that the samples had a certain crystalline quality. The results are in good agreement with that reported by Bushra and Ikhlas (2014). The crystallite size (D) was calculated by using the Scherer's equation (Reddy *et al.*, 2017):

$$D = 0.9\lambda/\beta\cos\theta \quad (1)$$

Where:

$\beta$ = A full-width at half maximum

$\lambda$ = The wavelength

Table 1: The obtained result of the XRD for pure and Ag-doped SnS films

| Ag-doped SnS (wt.%) | 2Θ (°) | hkl | FWHM (°) | Crystallite size (nm) |
|---|---|---|---|---|
| 0 | 30.60 | 101 | 2.3015 | 3.3313 |
| | 31.71 | 111 | 2.4103 | 3.1723 |
| | 45.72 | 002 | 1.0564 | 6.9336 |
| 0.002 | 30.57 | 101 | 1.7600 | 4.3565 |
| | 31.65 | 111 | 1.8429 | 4.1496 |
| | 45.67 | 002 | 0.8076 | 9.0713 |
| 0.004 | 30.52 | 101 | 1.5344 | 4.9976 |
| | 31.61 | 111 | 1.6062 | 4.7616 |
| | 45.63 | 002 | 0.7036 | 10.4137 |
| 0.006 | 30.45 | 101 | 0.3836 | 19.9938 |
| | 31.55 | 111 | 0.4021 | 19.0233 |
| | 45.57 | 002 | 0.1764 | 41.5459 |

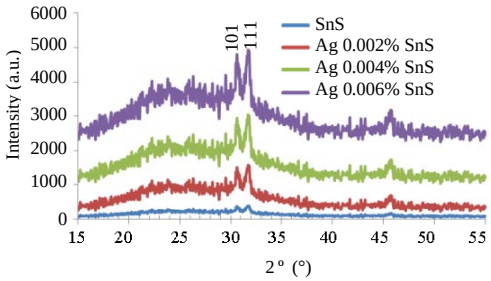


Fig. 1: The XRD spectrum of SnS and SnS:Ag films

The crystallite size increased with increasing of Ag doping for pure and Ag-doped SnS. The crystallite size of peak 111 increased from 3.1723-19.0233 nm. These results are in agreement with the researchers by Bushra and Ikhlas (2014). The results refer to the confinement effect. The results are listed in Table 1.

The shape and size of the prepared samples were determined by SEM. The deposition of pure and Ag-doped SnS on glass substrate for the samples are shown in Fig. 2. These figures show that the undoped and Ag-doped SnS film exhibits a smooth surface and free of pinholes consisting of small spherical grain size particles and increasing of Ag Nanoparticles size (NPs). It is clear from these micrographs that the surface morphology of the SnS films seems to be influenced by the Ag-doping. From figures show that increasing in Ag nanoparticle at some places the few clusters of NPs indicated the regular distribution free of holes and defects of nanoparticles during the deposition procedure.

This figures show the magnified view and the spherical morphology is evident which revealed the interesting distribution of triangle shaped nano particles. A few of the particles appeared larger while most of the particles were of same size. In a magnified view of Fig. 2a-d of pure and Ag-doped SnS it can be seen that the films have good symmetry. However, few larger spherical and near-spherical objects were also present which could be the result of the regular distribution free

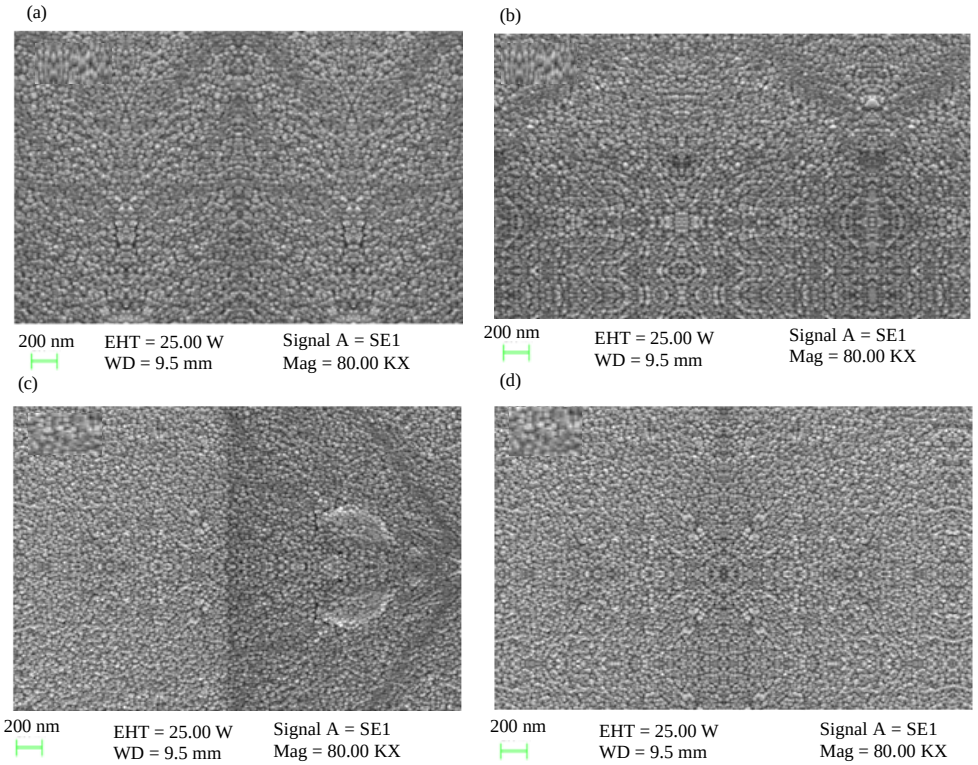


Fig. 2: SEM images of the undoped and SnS doped with different concentration with Ag thin films at thickness 75 nm: a) Pure SnS; b) SnS:0.002Ag; c) SnS:0.004Ag and d) SnS:0.006Ag

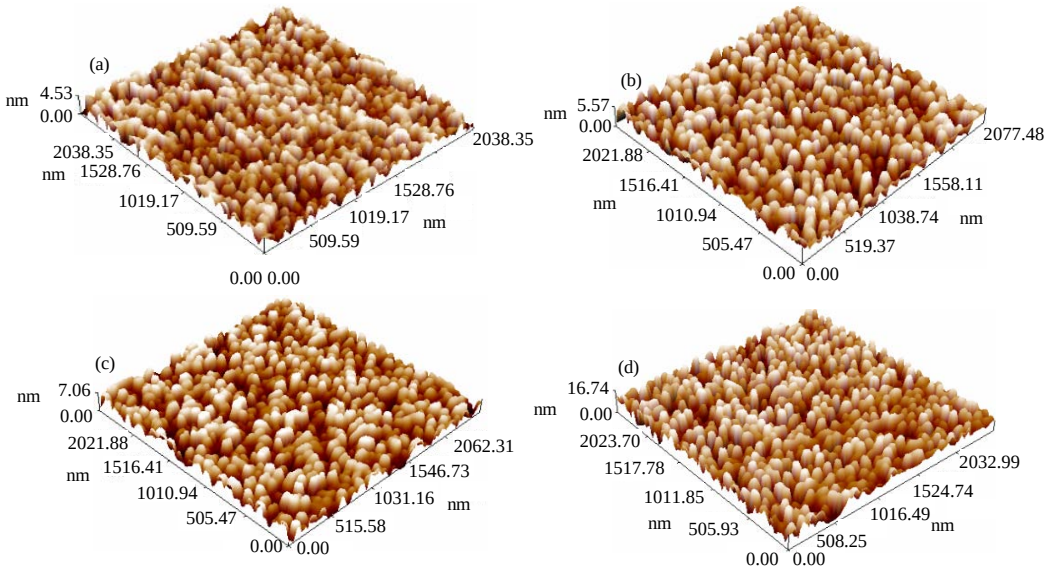


Fig. 3: 3D AFM images of: a) Pure; b) SnS:0.002% Ag; c) SnS:0.004% Ag and d) SnS:0.006% Ag films

of holes and defects of particles at some places on the glass substrate. The size measurement showed that these particles size from 15-65 nm which is in accordance with the findings of researches by Dehimi *et al*. (2015).

The AFM images of pure and Ag-doped SnS with different Ag-doping (0.002, 0.004, 0.006) wt.% thin films are presented in Fig. 3. The AFM images show a uniform granular surface morphology. From Fig. 3, it can observe

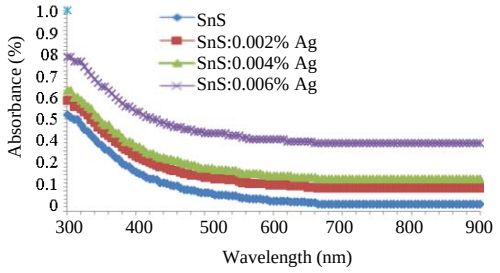


Fig. 4: The absorbance spectra as a function of wavelength of SnS:Ag films at different Ag-doping

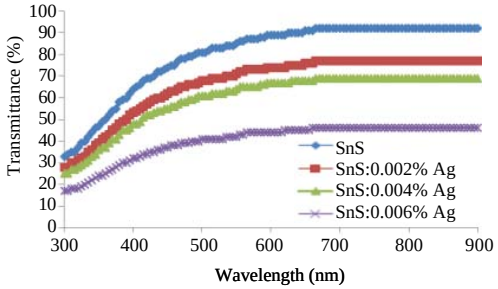


Fig. 5: Transmittance spectra as a function of wavelength of SnS:Ag films at different Ag-doping

Table 2: Morphological characteristics of SnS:Ag thin films deposited at different doping concentration

| Ag-doped (wt.%) | Roughness average Sa. (nm) | Root mean square Sq. (nm) | Ten point height Sz. (nm) | Average diameter (nm) |
|---|---|---|---|---|
| 0 | 1.00 | 1.18 | 2.67 | 73.87 |
| 0.002 | 1.27 | 1.48 | 3.21 | 79.97 |
| 0.004 | 1.54 | 1.82 | 4.32 | 81.91 |
| 0.006 | 3.58 | 4.23 | 9.45 | 94.39 |

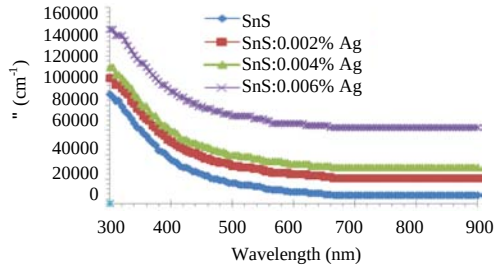


Fig. 6: The absorption coefficient spectra as a function of wavelength of SnS:Ag thin films at different Ag-doping

that the roughness increased from 1 nm for pure SnS (Fig. 3a) to 3.58 nm of SnS:0.006% Ag (Fig. 3d) films, these increases could be probably due to the increasing concentration of atomic silver nanoparticle in the SnS thin films.

The Root Mean Sequare (RMS) increased from 1.18 nm for pure SnS to 4.23 nm for SnS:0.006% Ag thin films which is in accordance with the findings of researches by Dehimi *et al*. (2015) and Tanusevskia and Poelmanb (2003). The average grain diameter was evaluated from the plane view images that increased from 73.87 nm for pure SnS to 94.37 nm for SnS: 0.006% Ag thin films. The tilted image exposes grain heights of a few tens of nanometers as shown in Table 2.

The optical properties of the pure and Ag-doped SnS with different Ag-doping (0.002, 0.004, 0.006) wt.% films are study from recording the absorbance spectra in the wavelength range 300-900 nm. It is possible to determine optical properties such as transmittance, absorption coefficient ($\alpha$), optical energy gap ($E_g$), refractive index (n), real and imaginary dielectric constant ($\varepsilon_r$, $\varepsilon_i$) by analyzing absorbance spectrum. Figure 4 represents the relationship between the absorbance spectra and wavelength of pure and Ag-doped SnS films with different Ag-doping. From Fig. 4, it can be observed that the absorbance was increase with the increasing of Ag-doping for the prepared films.

In addition, it can be observe that the transmittance decreased with increasing of Ag-doping in the SnS:Ag films as shown in Fig. 5 which is in agreement with the findings of researchers by Abdelrahman *et al*. (2012). The absorption coefficient ($\alpha$) of SnS:Ag thin films are calculated by using Eq. 2 (Marien *et al*., 2000):

$$\alpha = 2.303\ A/t \quad (2)$$

Where:
A = The absorbance
t = The film thickness

The absorption coefficient is determined from the region of high absorption at the fundamental absorption edge of the film. The variation of the absorption coefficient versus wavelength for pure and Ag-doped SnS with different Ag-doping (0.002, 0.004, 0.006) wt.% with annealing temperature 473 K at 2 h is presented in Fig. 6. It can be observed that the absorption coefficient is increase with increasing of Ag-doping. Its values are larger than ($10^4$/cm) which causes the increase of the probability of the occurrence direct transitions. This can be linked with the increase in grain size which is in agreement with the finding of researcher by Kafashan *et al*. (2016). The optical energy gap for SnS:Ag films is calculated by using Eq. 3 (Pankove, 1971):

$$(\alpha h\upsilon)^2 = [h\upsilon - E_g] \quad (3)$$

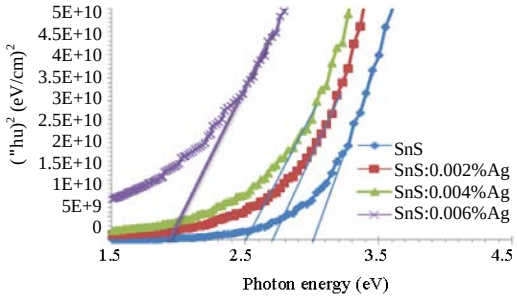


Fig. 7: A plots of $(\alpha h\upsilon)^2$ versus photon energy ($h\upsilon$) of SnS:Ag films at various Ag-doping

The plot of $(\alpha h\upsilon)^2$ with energy ($h\upsilon$) indicates that SnS films are direct transition. The band gap of the material is determined by extrapolating the linear region of the graph to the $h\upsilon$ axis. The curve can be fitted with straight line very well for a higher energy. Figure 7 shows the energy gap of pure and Ag-doped SnS with various Ag-doping (0.002, 0.004 and 0.006) wt.%. An obvious decreased is observed in the values of the energy gap with the increasing of Agdoping. This decreased in energy gap can be due to the prohibited impurities that led to the formation of donor levels within the energy gap near the conduction band. Thus, it will absorb photons of low energy. These results show a good agreement with the findings of researchers by Kafashan *et al*. (2016), Pankove (1971) and Wu *et al*. (2011). The refractive index (n) for SnS:Ag thin films is determined by using Eq. 4 (Mathews *et al*., 2010):

$$n = \left(\frac{4R}{(R-1)^2} - k^2\right)^{\frac{1}{2}} + \frac{(R+1)}{(R-1)} \quad (4)$$

Where:

k = The extinction coefficient

R = The reflectance

Figure 8 represents the relationship between the refractive index and the wavelength. From Fig. 8, it can notice that the refractive index increased with the increasing of Ag-doping in the wavelength range 400-900 nm. An increase in the particles congestion of the SnS film increase the refractive index. In other words, when the incident light interacts with a material which has a high amount of particles then the refractivity of the films increase. This is in agreement with. The real ($\varepsilon_r$) and imaginary ($\varepsilon_i$) parts of dielectric constant of SnS:Ag films was determined by using Eq. 5 and 6 (Nnabuchi, 2006):

$$\varepsilon_r = n^2 - k^2 \quad (5)$$

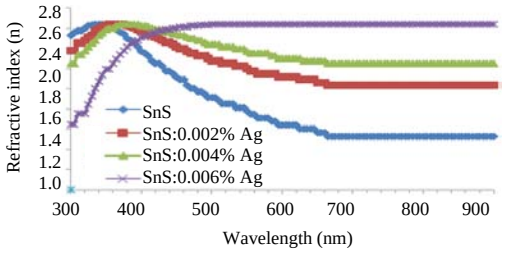


Fig. 8: Variation of extinction coefficient with wavelength of SnS:Ag films at various Ag-doping

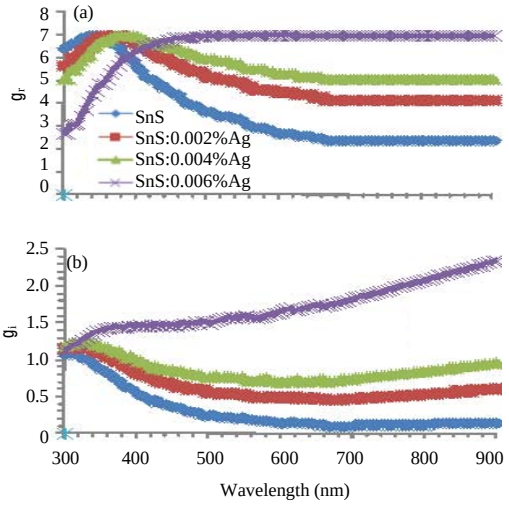


Fig. 9: Variation of a) $\varepsilon_r$ and b) $\varepsilon_i$ with wavelength of SnS:Ag films at various Ag-doping

$$\varepsilon_i = 2nk \quad (6)$$

From Fig. 9, we can observe that the $\varepsilon_r$ and $\varepsilon_i$ increased with increasing of Ag-doping for the prepared films. The Hall parameters such as Hall coefficient ($R_H$), carrier concentrations (n), electrical conductivity ($\sigma$) and Hall mobility ($\mu_H$) have been determined by using (Van-der Pau) system that tabulated in Table 3. It is obvious that the Hall coefficient decreased with increasing of Ag-doping. However, the carrier concentration of the samples increased with increasing of Ag-doping. In addition, the carrier concentration of the samples is positive which indicates that the SnS:Ag films are of p-type conduction. Therefore, Ag-doping can increase the carrier concentration which is in accordance with the findings of researchers by Lu *et al*. (2009) and Guneri *et al*. (2010). The electrical conductivity of SnS and Ag-doped SnS thin films increased with increasing Ag-doping which explained by increase in carrier concentration. The Hall mobility of SnS and Ag-doped SnS films decreased with increasing of Ag-doping, the

Table 3: The result of Hall measurement for Ag-doped SnS films

| Ag-doped SnS (wt.%) | $R_H$ ($cm^2$/C) | Carrier types | n/$(cm)^3$ | σ (1/Ω.cm) | $\mu_H$ ($cm^2$/V.sec) |
|---|---|---|---|---|---|
| 0.000 | $-7.919\times10^{7}$ | p | $3.058\times10^{11}$ | $1.940\times10^{-4}$ | $4.860\times10^{2}$ |
| 0.002 | $-2.608\times10^{7}$ | p | $5.433\times10^{11}$ | $6.480\times10^{-4}$ | $3.949\times10^{2}$ |
| 0.004 | $-1.014\times10^{7}$ | p | $6.195\times10^{11}$ | $1.678\times10^{-3}$ | $2.093\times10^{2}$ |
| 0.006 | $-9.555\times10^{5}$ | p | $7.169\times10^{11}$ | $2.011\times10^{-3}$ | $1.657\times10^{2}$ |

Table 4: The results of the I-V for Ag-doped SnS film at variou Ag-doping and temperature of 473 K

| Ag-doped SnS (wt.%) | $I_{sc}$ (mA/$cm^2$) | $V_{oc}$ (volt) | $I_{max}$ (mA) | $V_{max}$ (volt) | FF | η(%) |
|---|---|---|---|---|---|---|
| 0 | 3.6 | 2.8 | 1.60 | 1.1 | 0.17 | 1.76 |
| 0.002 | 7.4 | 2.5 | 1.60 | 1.7 | 0.14 | 2.72 |
| 0.004 | 4.9 | 2.5 | 2.10 | 2.00 | 0.34 | 4.2 |
| 0.006 | 7.0 | 2.5 | 1.70 | 1.60 | 0.25 | 4.42 |

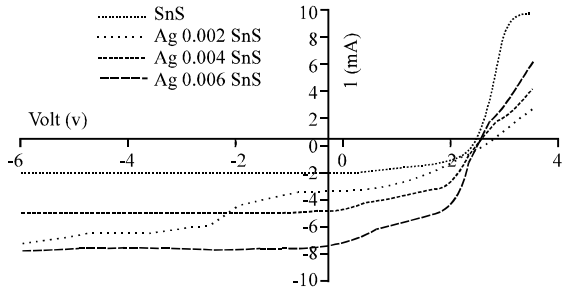


Fig. 10: I-V characteristic for pure Ag-doped SnS films under p = 100 mW/$cm^2$

decreased mobility of carriers caused by high carrier concentration which is in accordance with the findings by Lu *et al*. (2009) and Guneri *et al*. (2010).

The junction SnS:Ag/n-Si is formed by thermal evaporation technique and experimental by I-V curves which are of various behaviors according to the ambient of preparing the junction presented in Fig. 10. Hall measurements show that the pure SnS and SnS:Ag with Ag-doping (0.002, 0.004, 0.006) wt.% are p-type semiconductors. Anisotype p-n Heterojunction (HJ) will be obtained by SnS:Ag/n-Si for (0.002, 0.004, 0.006) wt.% because SnS:Ag are p-type and Si is n-type. The I-V curves of SnS:Ag/n-Si heterojunction are explained in Fig. 10 for illuminated conditions. The I-V characteristic for SnS:Ag/n-Si HJ at forward bias voltage for different Ag-doping within the range (-6 to 4 Volt). These curves exhibit the behavior of the current with the forward and reverse bias voltage. The current-voltage characteristic under illumination is one of the optoelectronic typical for HJ. The measurements are passed out under incident power densities equal to (100 mW/$cm^2$).

From Fig. 10, it is obvious that the photocurrent is increased with the increasing of bias voltage also it can be seen that the photocurrent in the reverse bias is larger than that in the forward bias. This can be attributed to the fact that the width of the depletion region increased with the increasing of the applied reverse bias voltage that leads to the separation of the electron-hole pairs.

The efficiency increased with increasing of Ag-doping can be obtained with an increase in Ag-doping from 0.002-0.006 wt.%. The highest efficiency at doping 0.006 wt.% is 4.42% with open circuit voltage ($V_{oc}$) of 2.5 V, short circuit current ($I_{sc}$) of 7 mA.$cm^{-2}$ and Full Factor (F.F) of 0.25. The improved device performance is caused by the high $I_{sc}$ and $V_{oc}$ of this device. The results are listed in Table 4.

The increased in efficiency is hence related to the scattering from Ag nanoparticles. Larger metal nanoparticles results in more scattering. This increases the optical path of incident light within the cell leading to more charge carriers being released.

## CONCLUSION

From XRD examination the polycrystalline SnS:Ag films are satisfied with orthorhombic structure and preferential orientation in the 111 direction, the crystallite size increased with the increasing of Ag-doping where increased from 3.1723 nm to 19.0233 nm in the 111 direction. SEM micrographs and AFM images showed that the film morphology and surface roughness were affected by low Ag-doping, from SEM particle size increased from 15-65 nm by increasing the Ag-doping, while from AFM, the roughness average and the Root Mean Square (RMS) are increased with the increasing of Ag-doping. The optical properties results show that the transmittance is decreased with the increasing of Ag-doping for the prepared films while the absorbance increased. The optical measurement shows that the pure and Ag-doped SnS films have allowed direct Energy gap ($E_g$) that decrease from 3-2 eV. Hall measurements indicate that SnS and Ag-doped SnS films are p-type semiconductors and found that the carrier concentration and electrical conductivity increased with the increasing of Ag-doping while the mobility decreased. The high conversion efficiency was 4.42% for 0.006% Ag-doped SnS thin film.

## REFERENCES


Abdelrahman, A.E., W.M.M. Yunus and A.K. Arof, 2012. Optical properties of tin sulphide (SnS) thin film estimated from transmission spectra. J. Non Cryst. Solids, 358: 1447-1451.

Avellaneda, D., G. Delgado and M. Nair, 2007. Physical properties of very thin SnS films deposited by thermal evaporation. Thin Solid Films, 515: 5771-5776.

Blaesser, G. and E. Rossi, 1988. Extrapolation of outdoor measurements of PV array I-V characteristics to standard test conditions. Solar Cells, 25: 91-96.

Bushra, A.H. and H.S. Ikhlas, 2014. Structural and optical properties of SnS thin films. J. Nanotechnol. Adv. Mater., 2: 43-49.

Dehimi, M., T. Touam, A. Chelouche, F. Boudjouan and D. Djouadi *et al*., 2015. Effects of low Ag doping on physical and optical waveguide properties of highly oriented sol-gel ZnO thin films. Adv. Condens. Matter Phys., 2015: 1-10.

Ghosh, B., M. Das, P. Banerjee and S. Das, 2008. Fabrication of vacuum-evaporated SnS/CdS heterojunction for PV applications. Solar Energy Mater. Solar Cells, 92: 1099-1104.

Guneri, E., F. Gode, C. Ulutas, F. Kirmizigul and G. Altindemir *et al*., 2010. Properties of P-type SNS thin films prepared by chemical bath deposition. Chalcogenide Lett., 7: 685-694.

Hartman, K., J.L. Johnson, M.I. Bertoni, D. Recht and M.J. Aziz *et al*., 2011. SnS thin-films by RF sputtering at room temperature. Thin Solid Films, 519: 7421-7424.

Henry, J., K. Mohanraj, S. Kannan, S. Barathan and G. Sivakumar, 2013. Effect of selenium doping on structural and optical properties of SnS: SE thin films by electron beam evaporation method. Eur. Phys. J. Appl. Phys., 61: 1-4.

Henry, J., K. Mohanraj, S. Kannan, S. Barathan and G. Sivakumar, 2015. Structural and optical properties of SnS nanoparticles and electron-beam-evaporated SnS thin films. J. Exp. Nanoscience, 10: 78-85.

Kafashan, H., R. Ebrahimi-Kahrizsangi, F. Jamali-Sheini and R. Yousefi, 2016. Effect of Al doping on the structural and optical properties of electrodeposited SnS thin films. Phys. Status Solidi A, 213: 1302-1308.

Lu, P.M., H.J. Jia and S.Y. Cheng, 2009. Optical and electrical properties of SnS: Ag films as solar cell absorbers. Adv. Mater. Res., 60: 11-15.

Mariappan, R., M. Ragavendar and V. Ponnuswamy, 2011. Structural and optical characterization of SnS thin films by electrodeposition technique. Optica Applicata, 41: 989-997.

Marien, J., T. Wagner, G. Duscher, A. Koch and M. Ruhle, 2000. NB on (110) TiO2 (Rutile): Growth, structure and chemical composition of the interface. Surf. Sci., 446: 219-228.

Mathews, N.R., H.B. Anaya, M.A. Cortes-Jacome, C. Angeles-Chavez and J.A. Toledo-Antonio, 2010. Tin sulfide thin films by pulse electrodeposition: Structural, morphological and optical properties. J. Electrochem. Soc., 157: H337-H341.

Nnabuchi, M.N., 2006. Optical and solid state characterization of optimized manganese Sulphide thin films and their possible applications in solar energy. Pac. J. Sci. Technol., 7: 69-76.

Pankove, J.I., 1971. Optical Processes in Semiconductors. Dover Publications, Inc., New York, USA., Pages: 429.

Peng, H., L. Jiang, J. Huang and G. Li, 2007. Synthesis of morphologically controlled tin sulfide nanostructures. J. Nanopart. Res., 9: 1163-1166.

Reddy, K.R., N.K. Reddy and R.W. Miles, 2006. Photovoltaic properties of SnS based solar cells. Solar Energy Mater. Solar Cells, 90: 3041-3046.

Reddy, K.R., P.P. Reddy, R.W. Miles and P.K. Datta, 2001. Investigations on SnS films deposited by spray pyrolysis. Opt. Mater., 17: 295-298.

Reddy, T.S., B.H. Kumar and M.S. Kumar, 2017. Effect of annealing on the optical properties and photoconductivity of SnS thin film. AIP. Conf. Proc., 1832: 080043-1-080043-3.

Sajeesh, T.H., A.R. Warrier, C.S. Kartha and K.P. Vijayakumar, 2010. Optimization of parameters of chemical spray pyrolysis technique to get n and p-type layers of SnS. Thin Solid Films 518: 4370-4374.

Tanusevski, A. and D. Poelman, 2003. Optical and photoconductive properties of SnS thin films prepared by electron beam evaporation. Solar Energy Mater. Solar Cells, 80: 297-303.

Vidal, J., S. Lany, M. D'avezac, A. Zunger and A. Zakutayev *et al*., 2012. Band-structure, optical properties and defect physics of the photovoltaic semiconductor SnS. Appl. Phys. Lett., 100: 032104-1-032104-4.

Wu, C., L. Shen, H. Yu, Q. Huang and Y.C. Zhang, 2011. Synthesis of Sn-doped ZnO nanorods and their photocatalytic properties. Mater. Res. Bull., 46: 1107-1112.